IEEE Photonics Journal
An IEEE Photonics Society Publication

Open Access

Electrically Programmable All-Fiber Structured Second Order Optical Temporal Differentiator

Volume 7, Number 3, June 2015

Ruoxu Wang
Rui Lin
Ming Tang, Senior Member, IEEE
Hailiang Zhang
Zhenhua Feng
Songnian Fu
Deming Liu
Perry Ping Shum, Senior Member, IEEE

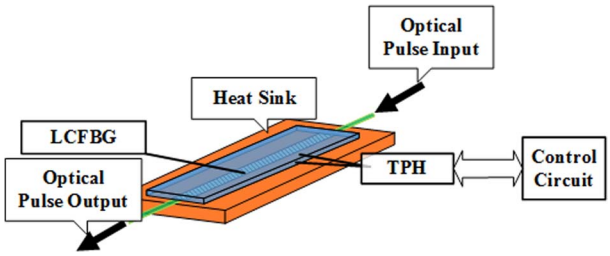

DOI: 10.1109/JPHOT.2015.2428245
1943-0655

IEEE photonics SOCIETY

IEEE

Electrically Programmable All-Fiber Structured Second Order Optical Temporal Differentiator

Ruoxu Wang,[1] Rui Lin,[1,2] Ming Tang,[1] *Senior Member, IEEE*, Hailiang Zhang,[3,4] Zhenhua Feng,[1] Songnian Fu,[1] Deming Liu,[1] and Perry Ping Shum,[3,4] *Senior Member, IEEE*

[1]National Engineering Laboratory for Next Generation Internet Access System, School of Optical and Electronic Information, Huazhong University of Science and Technology, Wuhan 430074, China
[2]School of Information and Communication Technology, KTH Royal Institute of Technology, 164 40 Stockholm, Sweden
[3]CINTRA CNRS/NTU/Thales, Unite Mixte Internationale 3288, Singapore 637553
[4]School of Electrical and Electronics Engineering, Nanyang Technological University, Singapore 637553

DOI: 10.1109/JPHOT.2015.2428245

Manuscript received January 12, 2015; revised April 26, 2015; accepted April 27, 2015. Date of publication April 30, 2015; date of current version May 18, 2015. This work was supported in part by the National 863 High-tech R&D Program of China under Grant 2013AA013402, by the National Natural Science Foundation of China under Grant 61331010 and Grant 61107087, by the Fundamental Research Funds for the Central Universities (HUST: 2013TS052), and by the Program for New Century Excellent Talents in University under Grant NCET-13-0235. Corresponding author: M. Tang (e-mail: tangming@mail.hust.edu.cn).

Abstract: We propose and experimentally demonstrate an electrically programmable second order optical temporal differentiator (OTD) based on linearly chirped fiber Bragg grating (LCFBG) and digital thermal print head (TPH). For the high-speed optical signal with 25-GHz repetition rate, an efficient second-order OTD has been achieved for arbitrary wavelength and bandwidth with the software-defined TPH configurations. By optimizing the thermooptic effect induced optical phase change in the LCFBG, the central wavelength of the differentiator can be reconfigured flexibly from 1543.5 to 1561.7 nm, with a step size of 0.114 nm. By dynamically controlling the heating elements bonded with the LCFBG, optical pulses with 0.55- and 0.8-nm 3-dB bandwidths have been successfully processed with acceptable deviation compared with the theoretical calculations.

Index Terms: Ultrafast device, pulse shaping, fiber gratings.

1. Introduction

To address the overwhelming demand for information transmission speed and operation bandwidth, signal processing in the optical domain has been proposed to overcome the electronics bottleneck [1]–[4]. Processing ultra-fast temporal signal all-optically can omit the opto-electronic conversion and take advantage of the large bandwidth of optical devices. For this purpose, all-optical signal processors, such as optical pulse shapers [5], optical temporal differentiators (OTDs) [6], integrators [7], [8], and Hilbert transformers [9], have recently been developed for all-optical processing and communication systems. Specifically, an OTD is a fundamental function-block for all-optical processing, which provides the real-time derivation of arbitrary signals in the optical domain with the potential to increase processing speed and bandwidth.

In comparison with the first-order OTD, the achievement of higher order OTD [10], which could offer more complex temporal waveforms, would be even more interesting. Several schemes of second-order OTDs have been previously proposed theoretically and experimentally, such as cross-gain modulation in semiconductor optical amplifiers (SOAs) [11], directional coupler [12], silicon based micro-ring resonator [13], interferometers [14], fiber Bragg gratings (FBGs) [15], or π-shift long period gratings (LPGs) [16], etc. In comparison with other methods, the fiber grating based OTDs have advantages of low cost, low losses, and fully compatible with fiber optical communication system. However, most of previous fiber grating based methods have fixed operation wavelength and pre-defined bandwidth for specific optical signal differentiation, thus they are not smart enough to support future flexible optical network in which optical signal will be diverse in not only operation wavelength but also pulse bandwidth. Therefore, it is essential to establish an adaptive OTD technology that owns reconfigurable capability for any incoming optical signals with alterable wavelength and bandwidth.

Recently, we have proposed and demonstrated a wavelength-tunable second-order optical temporal differentiator with wavelength tunability [17]. The central wavelength of the differentiation can be reconfigured from 1556.4 to 1560.3 nm. The optical pulses being processed are coming from a low repetition rate (tens of MHz) mode-locked fiber laser and the bandwidth of the pulse is fixed. Programmable OTD for real communication signal (repetition rate larger than 10 GHz) has yet to be investigated. More importantly, an OTD with reconfigurable operation bandwidth will be more meaningful for optical signals with different pulse-width and the bandwidth tunability is very difficult to achieve with previously published arts. In this paper, we proposed and experimentally demonstrated a programmable wavelength-tunable and bandwidth-adaptable second-order OTD for high-speed signal with different bandwidth and wavelength. The OTD is based on a linearly chirped fiber Bragg grating (LCFBG) and a thermal printer head (TPH) controller. The fully digital controlled TPH provides a dense thermal array that can precisely configure the temperature point-by-point. With tight bonding and responsible thermal management, the local phase change along the all-fiber structured LCFBG can be easily tailored by the thermo-optical effect. By using in-house developed computer controlled thermo-control circuits, the thermo-optical effect induced phase change and filtering function can be conveniently programmed electrically and combined to achieve OTD performance for versatile wavelength and pulse bandwidth.

The rest of this paper is organized as follows. The principle and configuration of the second-order temporal differentiator based on an LCFBG and digital thermal controller is described in Section 2. In Section 3, the experiment of second-order optical temporal differentiation is implemented. Then the reconfigurable capability for different wavelength and 3-dB pulse bandwidth has been achieved and analyzed in Section 4. A second-order OTD with the central wavelength tunable from 1543.5 nm to 1561.7 nm and the operation bandwidth optimized for 0.55 nm and 0.8 nm is experimentally demonstrated and discussed. A conclusion is drawn in Section 5.

2. Principle and System Configuration

An Nth-order optical temporal differentiator $(N = 1, 2 \ldots)$ can provide Nth-time derivative of any complex envelope of an input optical signal waveform. We assume that the Nth-order differentiator can be expressed as

$$u_{\text{out}}(t) = \partial^N u_{\text{in}}(t)/\partial t^N \tag{1}$$

where $u_{\text{in}}(t)$ is the complex envelope of an input optical signal and $u_{\text{out}}(t)$ is the Nth-time derivative of the complex envelope.

We can express (1) in frequency domain as

$$U_{\text{out}}(\omega - \omega_0) = [j(\omega - \omega_0)]^N U_{\text{in}}(\omega - \omega_0) \tag{2}$$

where ω and ω_0 are the optical frequency variable and the central optical frequency, U_{out} and U_{in} are the spectral function of $u_{\text{out}}(t)$ and $u_{\text{in}}(t)$, respectively.

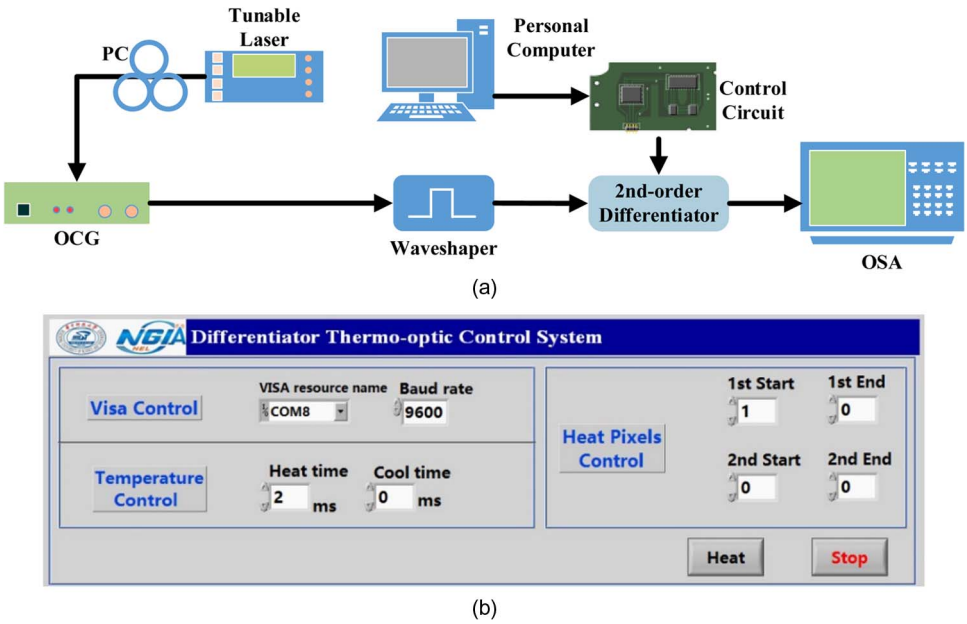

Fig. 1. (a) Experimental setup of the second order optical temporal differentiator system. (b) Software control panel.

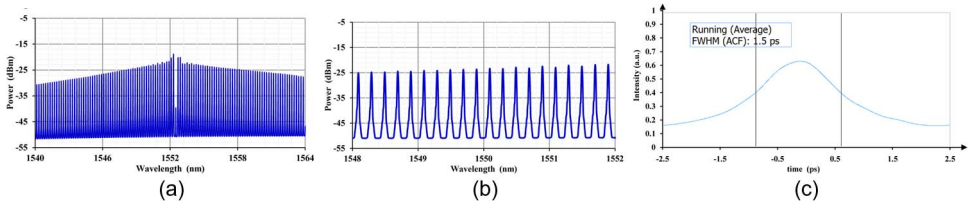

Fig. 2. Optical comb generator output. (a) Optical spectrum. (b) Local spectrum from 1548 to 1552 nm. (c) Time-domain waveform.

It is obviously shown in (2) that the spectrum transmission function of an *N*th-order differentiator can be given by

$$H_{\text{diff}}(\omega-\omega_0) = U_{\text{out}}(\omega-\omega_0)/U_{\text{in}}(\omega-\omega_0) = [j(\omega-\omega_0)]^N. \tag{3}$$

It is easily seen that for the even-order differentiator such as second-order or fourth-order, the response of the transmission function should only depend on the amplitude without an extra π phase shift.

The proposed experimental system to implement the second-order optical temporal differentiator is shown in Fig. 1. In previous work [17], we used a relatively low repetition rate (558 MHz) mode-locked fiber laser to generate the input pulse, and the operation frequency and the pulse bandwidth cannot be adjusted. In this paper, the mode-locked fiber laser has been replaced with a tunable continuous wave laser combined with an optical comb generator (OCG) to produce a higher repetition rate optical pulse train. The linewidth of the tunable laser (IDPhotonics, CBDX4) is less than 100 kHz and the OCG (OptoComb, WTAS-02) has a repetition rate of 25 GHz. A polarization controller (PC) is placed between the tunable laser and the OCG to control the polarization state for optimized comb generation.

The spectral and temporal output from the comb generator are shown in Fig. 2. The optical spectrum was measured by an optical spectrum analyzer (OSA) (YOKOGAWA, AQ6370C) and the optical pulse time domain waveform was recorded by an autocorrelator (APE,

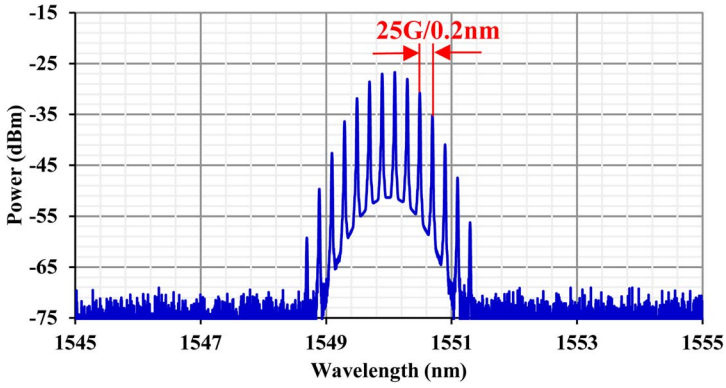

Fig. 3. Output optical spectrum after the waveshaper.

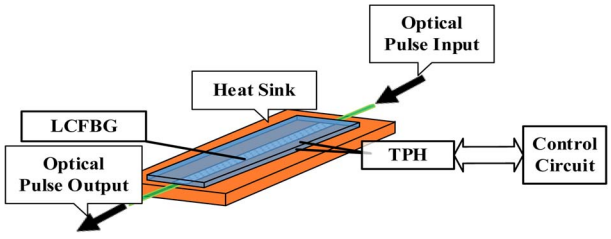

Fig. 4. Construction of the second-order optical differentiator.

Pulse-Check50). As Fig. 2(c) shows, the output of the OCG is a picosecond (FWHM is 1.5 ps) optical pulse train in time domain with 25 GHz repetition rate.

After the comb generation stage, we use a waveshaper (Finisar, Waveshaper4000S) to carve the optical spectrum of the OCG output. Due to the wide wavelength range of the OCG output and flexible functions provided by waveshaper, optical pulses with arbitrary central wavelength and adjustable bandwidth can be easily obtained for the subsequent process. As an example, a Gaussian shape spectral transfer function is configured within the waveshaper and the output of OCG can be modified to a Gaussian-like optical spectrum as shown in Fig. 3.

The pre-shaped Gaussian-like pulse after the waveshaper is injected into our proposed programmable second-order optical differentiator. The second-order differentiator consists of LCFBG and TPH that is driven and controlled by our in-house built driving circuit. The monolithic optoelectronic system is connected with personal computer via USB-RS232 cable to implement the data interaction. A LabView-based software (as the control panel in Fig. 1(b) shows) is developed to control and monitor the performance of the differentiator conveniently. Since the output optical pulse bandwidth is far beyond our photodetector and oscilloscope bandwidth, we use an optical spectrum analyzer (OSA) (YOKOGAWA, AQ6370C) to retrieve the spectrum information and conduct the time-domain analysis through the inverse Fourier transform before and after differentiation.

The detailed construction of our second-order optical differentiator is shown in Fig. 4. A programmable TPH is fixed tightly with a LCFBG. The optical pulses to be processed propagate along the LCFBG in the transmission direction. The whole unit is connected with a heat sink that can alleviate unwanted heat diffusion brought by the TPH and improve the stability and precision of the processing capacity for the monolithic optoelectronic circuit.

It has been proven that a phase shift will be generated when a specific position of an LCFBG is heated [20]. The magnitude of the phase shift is given by

$$\phi = \frac{2\pi L}{\lambda}\beta\Delta T \tag{4}$$

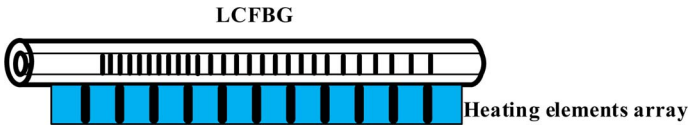

Fig. 5. Construction of the contact area between the heating pixels array and the LCFBG.

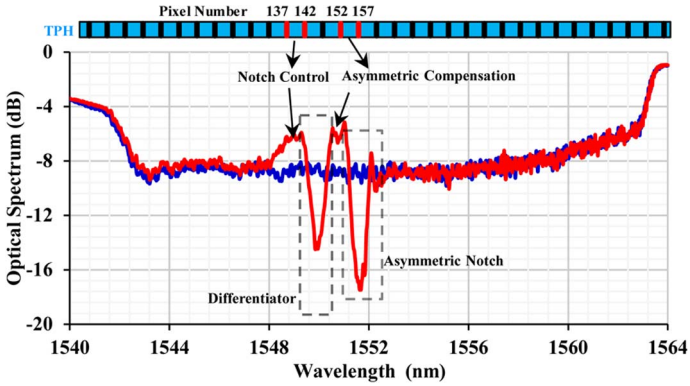

Fig. 6. Transmission spectrum of the LCFBG with/without heat. The blue curve is the original transmission spectrum without heat, and the red curve is after heat.

in which ϕ is the phase shift, L is the length of the heating region, β is the thermo-optical coefficient, which is around 8.6×10^{-6} K^{-1} in silica fiber, and ΔT is the temperature change.

In the transmission spectrum of the LCFBG, the introduced phase shift will result in a narrow transmission window in the stop band due to destructive interference of the reflected light. At the same time, if the heating length is applied longer than the grating pitch (that is usually the case), a transmission notch will appear besides the longer wavelength of the transmission peak [18]. On the other hand, the wavelength of the phase shift can be determined by the heating position. A programmable optical spectral waveshaper is then constructed to arbitrarily alter the wavelength and bandwidth of transmission notch by controlling the heating profiles [19]. With this principle, a second-order optical differentiator can be achieved with carefully configured transmission spectrum at desired wavelength and suitable bandwidth.

In our experiment, a commercialized thermal print head (manufactured by Fujitsu, model No. FTP628MCL701), is used and this model consists of 384 heating pixels array with spacing of 125 μm between each pixels, and the total length of the TPH is 48 mm. The power consumption of the TPH based thermo-control circuit is about 7.5 W with 5 V driving voltage and 1.5 A average working current. The LCFBG is 24 mm long, 3 dB bandwidth is 21.2 nm from 1541.8 to 1563 nm. The heating array and the LCFBG are firmly contacted with each other to guarantee good heating conduction. The detailed construction is shown in Fig. 5.

3. Implementation of the Second Order Differentiator

By using a broadband light source (BLS), the original transmission spectrum of the LCFBG without heating is shown by the blue curve in Fig. 6. When two separated regions of the LCFBG are heated simultaneously, two transmission peaks are appeared with a deeply concave region between the two peaks. The notch filtering region as illustrated by red curve in Fig. 6 can be used to perform the differentiation operation. It is worth mentioning that the purpose of heating two independent regions is to keep balance of both sides of the differentiator notch. The left heated region controls the notch's position and basic shape, and the right heated region is as for asymmetric compensation. If only heating the left region, two sides of the notch will be asymmetrical as shown by the second notch in Fig. 6 and it will deteriorate the device performance.

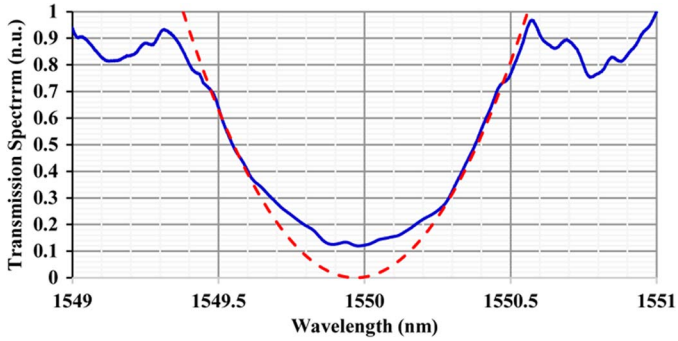

Fig. 7. Normalized local transmission spectrum of the second order differentiator. The blue curve is the real output spectrum, and the red dashed curve is the ideal transmission function.

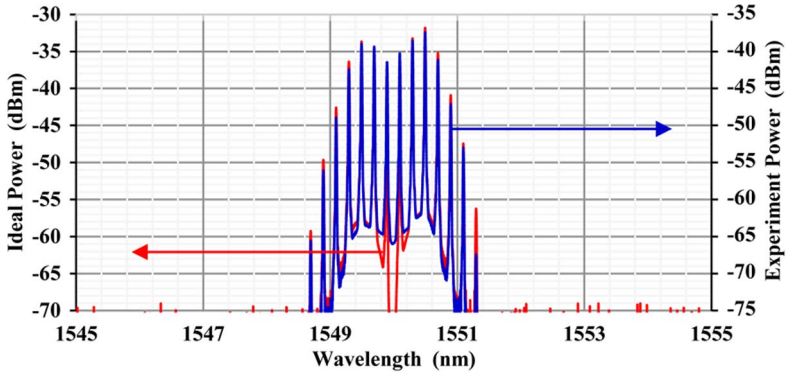

Fig. 8. Optical spectrum of the output pulse signal after second order differentiation (blue curve) and ideal spectrum (red curve).

Since our system is fully programmable with computer software control, a suitable transmission spectrum for second-order differentiation can be easily obtained. For example, an ideal second-order optical temporal differentiator's transmission function is depicted in Fig. 7 with the central wavelength at 1550 nm and 3-dB bandwidth at 0.8 nm. In order to represent this transmission spectrum in practice, two heating regions (pixels 137–142 and 152–157) are activated. Each region has 6 pixels in length (0.75 mm) and the unheated spacing between two heated areas is 9 pixels in length (1.125 mm). With this heating profile (sandwiched heated + unheated + heated pixels are: 6 + 9 + 6), the experimentally realized second-order differentiator transmission function curve is shown in Fig. 7 with blue curve. The experimental result matches the ideal curve very well.

With this configuration, a Gaussian-like optical pulse generated by OCG and Finisar waveshaper is differentiated and the spectrum of the output optical pulse signal is demonstrated in Fig. 8. The red line is the ideal second-order differentiated output spectrum and the blue line is the experimental result. The experimental spectrum coincides with the theoretical calculation quite well with 5dB less in power that is attributed to the insertion loss of the OTD system.

By taking inverse fast Fourier transform (IFFT) of the signal spectrum, temporal waveform of optical signal before and after OTD can be obtained. As shown in Fig. 9, the dotted green curve is the normalized time-domain waveform of the input Gaussian-like pulse signal and the solid blue curve is the experimental output waveform after second order OTD. For comparison, the ideal second order differentiation of the input optical pulse is also plotted in Fig. 9 with dashed red curve. The deviation, which is calculated by

$$D = \sum_{-N/2}^{N/2} \frac{|f_{exp} - f_{ideal}|}{f_{ideal}} \tag{5}$$

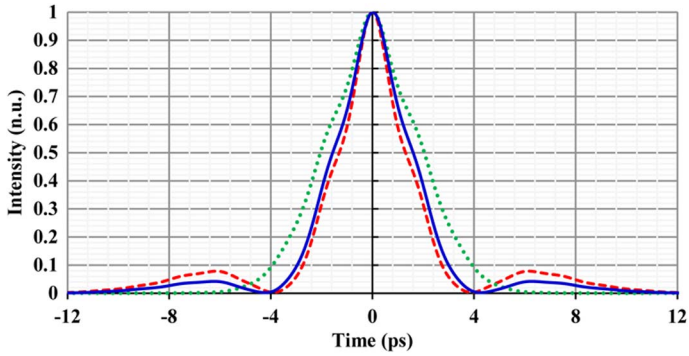

Fig. 9. Time domain waveforms of the optical pulse. The green dotted curve is input Gaussian-like pulse, the red dashed curve is the ideal second order differentiator, and the blue solid curve is the experimental output waveform of the second order differentiator.

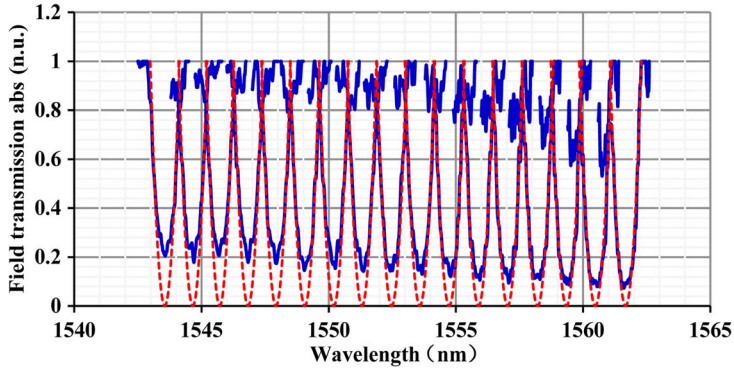

Fig. 10. Least square method fitting of the second order differentiator spectrum.

where N is the IFFT point, f_{exp} and f_{ideal} represent the experimental value and ideal value between the experimental output time-domain waveform of the second-order differentiator, and the ideal second order differentiation waveform is about 12.41%, which indicates that our differentiator is quiet accurate for implementation of second order differentiation.

4. Wavelength Tunable and Bandwidth-Adaptable OTD

By taking the advantage of the programmable thermo-optic circuit, reconfigurable heating profile hence the transmission window can be accomplished for wavelength tunable and bandwidth adaptable OTD operation.

For the wavelength tunable OTD operation, we treat the heating structure adopted in Fig. 6 as a basic building block (the length of two heated regions is 0.75 mm and unheated interval between them is 1.125 mm) and scan the central position of the heating structure along the TPH/LCFBG with a step of 1.25 mm (10 pixels). It is anticipated that a wavelength-tunable second-order differentiator with fixed 3 dB bandwidth can be achieved. Fig. 10 shows the experimentally generated second-order differentiator transmission spectrum at 17 wavelengths with blue solid curves from 1543.5 to 1561.7 nm. The experimental transmission spectra were measured 17 times with the same heating profile but different heating positions. The red dash line indicates the curve fitted ideal second order OTD spectrum at 17 wavelengths. It is demonstrated that the difference between experimental result and the ideal second order differentiator is acceptable. The deviations of those 17 sets of data are calculated by

$$D_f = \sum_{0}^{n} |f_{efre} - f_{ffre}| \Big/ \sum_{0}^{n} f_{ffre} \tag{6}$$

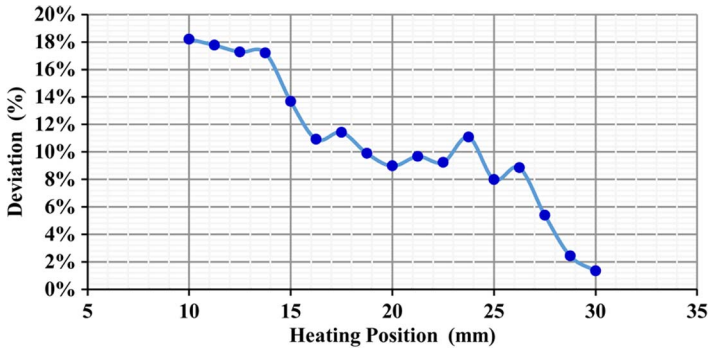

Fig. 11. Relationship between deviation and the heating position.

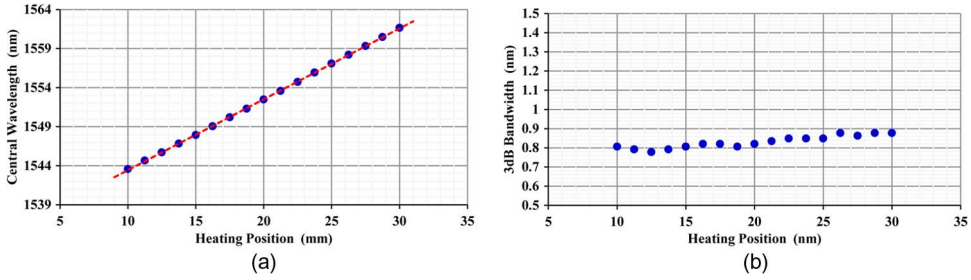

Fig. 12. Relationship between (a) central wavelength and (b) 3 dB bandwidth of the second order differentiator and the heating position. The blue dots in (a) and (b) are the experimental result, and the red dashed line in (a) is the linear fitting line.

and are shown in Fig. 11. In (6), D_f is the deviation, f_{efre} is the experimental data, f_{ffre} is the fitting curve value, and n is the number of sampling point in the spectrum. Relatively larger deviations observed in the shorter wavelength region result from lower extinction ratio of the notch filter accordingly. This phenomenon can be attributed to the undesirable cladding-mode loss in the fiber grating and can be easily overcome by using cladding-mode suppressed fibers in the fabrication of the LCFBG [20].

Since the FBG used in our work is linearly chirped, the local Bragg wavelength changes linearly with the position along the LCFBG axis. We can use the heating source to introduce a phase shift to break the local Bragg condition at specific position thus a transmission peak can be generated in the stopband. The transmission wavelength can be linearly changed as we scan the heating position along the LCFBG. Similarly, by designing a suitable heating profile and scanning the heating position along the LCFBG, the second order differentiator at different wavelength can be obtained and the central wavelength has a linear relationship with the heating position. In the experiment, we conducted the wavelength tuning operation and the relationship between the central wavelength of the second-order differentiator and heating position is shown in Fig. 12(a). A nearly perfect linear relationship can be observed and the slope of the linear fitting line is about 0.91 nm/mm. Since the pixel pitch of the heating array is 0.125 mm, the minimal wavelength adjustment step size is 0.114 nm per pixel. The wavelength tuning step size can be further refined by using lower chirp rate gratings. Fig. 12(b) shows the variation of the 3 dB bandwidth of OTD with the change of the central wavelength. Good stability can be found and the maximum deviation apart from 0.8 nm 3 dB bandwidth is 8.75%.

For the bandwidth adaptable OTD operation, we keep the central wavelength of the second-order differentiator constant while change the spacing between two heating regions to process the incoming optical pulses with different pulsewidth/bandwidth. When the central wavelength of the input optical pulse to the OTD is 1550 nm, we adjust the 3 dB bandwidth of input pulse from 0.1 nm to 1.4 nm. The operational bandwidth of our proposed OTD is also configured by

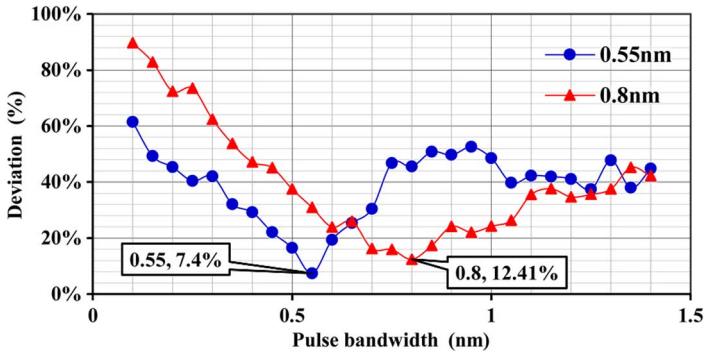

Fig. 13. Relationship between second order differentiator deviation and the 3-dB bandwidth of the input pulse, where the input pulse central wavelength is 1550 nm (spacing between two heated regions is 0.75 mm for the blue dot curve and 1.125 mm for the red triangle curve).

changing the heating conditions. The processed spectrum is captured, and the deviation is calculated by (5) and compared with the ideal spectrum, as demonstrated in Fig. 13. It can be found that, for 0.55 nm pulse bandwidth, the optimized second order OTD operation brings 7.4% deviation with a specific heating configuration (0.875 mm and 0.75 mm for two heating regions and the separation is 0.75 mm). For the input optical pulse with 0.8 nm bandwidth, 12.41% deviation can be achieved with a different heating configuration (0.75 mm for two heating regions and the separation is 1.125 mm). The results indicate that our proposed OTD can be adaptable to the incoming signal's bandwidth and fulfill the differentiation requirement by dynamically controlling the configurations of thermo-array.

It should be noted that although the response time of the TPH thermal element is less than 1.5 ms, the average reconfiguration time of our differentiator to different wavelength or bandwidth is about 500 ms, considering the heat-conduction time.

5. Conclusion

In this paper, we proposed and experimentally demonstrated an electrically programmable wavelength-tunable and bandwidth-adaptable second-order differentiator based on a linearly chirped fiber Bragg grating and digital controlled thermal print head with 384 heating pixels. The optical pulsed signal to be differentiated is generated by a tunable laser and an optical comb generator, and then pre-shaped by a waveshaper to become a Gaussian-like spectrum. The second-order differentiator operation wavelength can be easily configured from 1543.5 nm to 1561.7 nm with the step size of 0.114 nm per pixel. The 3 dB bandwidth of the differentiator is programmable to realize the minimized differentiation process for incoming high speed optical pulses (25 GHz repetition rate in this work) with different bandwidths. The experimentally achieved OTD for 0.55 nm and 0.8 nm signal bandwidth leads to the deviation of 7.4% and 12.41%, compared with the ideal transformation respectively, using the same device with software-defined configurations. With the development of qualified LCFBG and thermo-optical management, the technique established in this work is promising for future all-optical signal processing with reconfigurable features. It will be also interesting to explore a comprehensive heating strategy, together with suitable FBG to achieve higher order or odd-order OTD with accurate phase response control in the differentiator's transmission spectrum.

References

[1] R. S. Tucker, “The role of optics in computing,” *Nat. Photon.*, vol. 4, pp. 405–405, Jul. 2010.
[2] L. Venema, “Photonic technologies,” *Nature*, vol. 424, pp. 809–809, 2003.
[3] J. Azana, C. Madsen, K. Takiguchi, and G. Cincotti, “Guest editorial—Optical signal processing,” *J. Lightw. Technol.*, vol. 24, no. 7, pp. 2484–2486, Jul. 2006.

[4] M. R. Fernandez-Ruiz, A. Carballar, and J. Azana, "Design of ultrafast all-optical signal processing devices based on fiber Bragg gratings in transmission," *J. Lightw. Technol.*, vol. 31, no. 10, pp. 1593–1600, May 15, 2013.
[5] P. Petropoulos, M. Ibsen, A. D. Ellis, and D. J. Richardson, "Rectangular pulse generation based on pulse reshaping using a superstructured fiber Bragg grating," *J. Lightw. Technol.*, vol. 19, no. 5, pp. 746–752, May 2001.
[6] M. Li, D. Janner, J. P. Yao, and V. Pruneri, "Arbitrary-order all-fiber temporal differentiator based on a fiber Bragg grating: Design and experimental demonstration," *Opt. Exp.*, vol. 17, no. 22, pp. 19 798–19 807, Oct. 26, 2009.
[7] N. Q. Ngo, "Design of an optical temporal integrator based on a phase-shifted fiber Bragg grating in transmission," *Opt. Lett.*, vol. 32, no. 20, pp. 3020–3022, Oct. 15, 2007.
[8] M. Ferrera *et al.*, "On-chip CMOS-compatible all-optical integrator," *Nature Commun.*, vol. 1, Jun. 2010.
[9] M. H. Asghari and J. Azana, "All-optical Hilbert transformer based on a single phase-shifted fiber Bragg grating: Design and analysis," *Opt. Lett.*, vol. 34, no. 3, pp. 334–336, Feb. 1, 2009.
[10] R. Slavik, Y. Park, M. Kulishov, and J. Azana, "Terahertz-bandwidth high-order temporal differentiators based on phase-shifted long-period fiber gratings," *Opt. Lett.*, vol. 34, no. 20, pp. 3116–3118, Oct. 15, 2009.
[11] Z. Y. Li and C. Q. Wu, "All-optical differentiator and high-speed pulse generation based on cross-polarization modulation in a semiconductor optical amplifier," *Opt. Lett.*, vol. 34, no. 6, pp. 830–832, Mar. 15, 2009.
[12] M. Li, H. S. Jeong, J. Azana, and T. J. Ahn, "25-terahertz-bandwidth all-optical temporal differentiator," *Opt. Exp.*, vol. 20, no. 27, pp. 28 273–28 280, Dec. 17, 2012.
[13] J. J. Dong *et al.*, "High-order photonic differentiator employing on-chip cascaded microring resonators," *Opt. Lett.*, vol. 38, no. 5, pp. 628–630, Mar. 1, 2013.
[14] J. J. Dong *et al.*, "Compact, flexible and versatile photonic differentiator using silicon Mach–Zehnder interferometers," *Opt. Exp.*, vol. 21, no. 6, pp. 7014–7024, Mar. 25, 2013.
[15] M. A. Preciado, X. W. Shu, P. Harper, and K. Sugden, "Experimental demonstration of an optical differentiator based on a fiber Bragg grating in transmission," *Opt. Lett.*, vol. 38, no. 6, pp. 917–919, Mar. 15, 2013.
[16] J. Azana and M. Kulishov, "All-fibre ultrafast optical differentiator based on pi phase-shifted long-period grating," *Electron. Lett.*, vol. 41, no. 25, pp. 1368–1369, Dec. 8, 2005.
[17] H. L. Zhang *et al.*, "Programmable wavelength-tunable second-order optical temporal differentiator based on a linearly chirped fiber Bragg grating and a digital thermal controller," *Opt. Lett.*, vol. 39, no. 7, pp. 2004–2007, Apr. 1, 2014.
[18] I. Petermann, S. Helmfrid, O. Gunnarsson, and L. Kjellberg, "Tunable and programmable optical bandpass filter," *J. Opt. Pure Appl. Opt.*, vol. 9, no. 11, pp. 1057–1061, Nov. 2007.
[19] H. L. Zhang *et al.*, "Programmable all-fiber structured waveshaper based on linearly chirped fiber Bragg grating and digital thermal controller," *Appl. Phys. B-Lasers Opt.*, vol. 112, no. 4, pp. 479–484, Sep. 2013.
[20] S. Y. Li, N. Q. Ngo, S. C. Tjin, P. Shum, and J. Zhang, "Thermally tunable narrow-bandpass filter based on a linearly chirped fiber Bragg grating," *Opt. Lett.*, vol. 29, no. 1, pp. 29–31, Jan. 1, 2004.